Differentiation of Prostatitis and Prostate Cancer by Using Diffusion-weighted MR Imaging and MR-guided Biopsy at 3 T[1]

Klaas N. A. Nagel, BS
Martijn G. Schouten, MS
Thomas Hambrock, MD
Geert J. S. Litjens, MS
Caroline M. A. Hoeks, MD
Bennie ten Haken, PhD
Jelle O. Barentsz, MD, PhD
Jurgen J. Fütterer, MD, PhD

Purpose: To determine if prostatitis and prostate cancer (PCa) can be distinguished by using apparent diffusion coefficients (ADCs) on magnetic resonance (MR) images, with specimens obtained at MR-guided biopsy as the standard of reference.

Materials and Methods: The need for institutional review board approval and informed consent was waived. MR-guided biopsies were performed in 130 consecutive patients with cancer-suspicious regions (CSRs) on multiparametric MR images obtained at 3 T. In this retrospective study, 88 patients met the inclusion criteria. During the biopsy procedure, an axial diffusion-weighted sequence was performed and ADC maps were generated (repetition time msec/echo time msec, 2000/67; section thickness, 4 mm; in-plane resolution, 1.8 × 1.8 mm; and *b* values of 0, 100, 500, and 800 sec/mm^2). Subsequently, a confirmation image with the needle left in situ was acquired and projected on the ADC map. The corresponding ADCs at the biopsy location were compared with the histopathologic outcomes of the biopsy specimens. Linear mixed-model regression analyses were used to test for ADC differences between the histopathologic groups.

Results: The study included 116 biopsy specimens. Median ADCs of normal prostate tissue, prostatitis, low-grade PCa (Gleason grade components 2 or 3), and high-grade PCa (Gleason grade components 4 or 5) were 1.22 × 10^{-3} mm^2/sec (standard deviation, ± 0.21), 1.08 × 10^{-3} mm^2/sec (± 0.18), 0.88 × 10^{-3} mm^2/sec (± 0.15), and 0.88 × 10^{-3} mm^2/sec (± 0.13), respectively. Although the median ADCs of biopsy specimens with prostatitis were significantly higher compared with low- and high-grade PCa ($P < .001$), there is a considerable overlap between the tissue types.

Conclusion: Diffusion-weighted imaging is a noninvasive technique that shows differences between prostatitis and PCa in both the peripheral zone and central gland, although its usability in clinical practice is limited as a result of significant overlap in ADCs.

[1] From the Department of Technical Medicine (K.N.A.N.) and MIRA-Institute for Biomedical Technology and Technical Medicine, Neuroimaging Group (B.t.H.), University of Twente, Enschede, the Netherlands; and Department of Radiology, Radboud University Nijmegen Medical Centre, Geert Grooteplein 10, 6525 GA Nijmegen, the Netherlands (M.G.S., T.H., T.J.S.L., C.M.A.H., J.O.B., J.J.F.). Received August 11, 2011; revision requested September 27; revision received June 14, 2012; accepted August 16; final version accepted September 18. Supported by the Dutch Cancer Society. **Address correspondence to** J.J.F. (e-mail: *j.futterer@rad.umcn.nl*).

Urologists often face the dilemma of treating a patient in whom there is a high suspicion for prostate cancer (PCa) based on an elevated prostate-specific antigen (PSA) level (1–3). Benign prostatic hyperplasia can also lead to elevated PSA levels and is not always associated with clinical symptoms. Therefore, differentiation between PCa and benign prostatic hyperplasia in the central gland (CG) is a major challenge for the urologist and also for the radiologist. Prostatitis is normally a diffuse disease, whereas benign prostatic hyperplasia and tumor normally present as focal disease. Prostatitis can be a cause of an elevated PSA level; however, this is clinically a difficult diagnosis. As a consequence, prostatitis patients will undergo transrectal ultrasonography (US)–guided biopsy sessions. Moreover, PCa can still be present in patients with biopsy-proved prostatitis. This illustrates the need for a noninvasive diagnostic test that can be used to differentiate between PCa and prostatitis (4).

Magnetic resonance (MR) imaging of the prostate is the imaging modality of choice in PCa detection, localization, and staging (5–8). The diagnostic value of anatomic T2-weighted MR imaging in discriminating PCa from benign prostate tissue is limited. The interpretation of these images can be affected by false-positive findings such as prostatitis, postbiopsy hemorrhage, and fibrosis (9–11). To improve the diagnostic accuracy of prostate MR imaging, functional imaging techniques have been applied, such as dynamic contrast-enhanced MR imaging (12–14), proton MR spectroscopic imaging (15–17), and diffusion-weighted (DW) MR imaging (18–21), with limited success to date.

DW imaging has been shown to aid in distinguishing between malignant and benign prostate tissue based on relatively lower apparent diffusion coefficients (ADCs) of cancer tissue (22–35). The correlation between the ADC and tissue is usually done by using transrectal US-guided biopsy and step-section specimens after prostatectomy as a standard of reference (31–35). Even using improved correlation methods (35) there is still an uncertainty whether the correct tissue is sampled and correlated with imaging.

MR-guided biopsy may overcome the latter limitations. A confirmation MR image can be acquired with the needle left in situ. This allows for an accurate verification of the biopsy location in the cancer-suspicious region (CSR) and correlation with the ADC map. Therefore, the purpose of our study was to determine if prostatitis and PCa can be distinguished by using ADCs on MR images, with specimens obtained at MR-guided biopsy as the standard of reference.

Advances in Knowledge

- The median apparent diffusion coefficient (ADC) of prostatitis (1.08×10^{-3} mm^2/sec [standard deviation, ± 0.18]) differed from prostate cancer for both peripheral zone and central gland (0.88×10^{-3} mm^2/sec [standard deviation, ± 0.13 and 0.15]); however, substantial overlap exists.
- Diffusion-weighted imaging may help reduce the number of false-positive findings at prostate cancer MR imaging.

Implication for Patient Care

- The median ADCs for prostatitis and prostate cancer differed in our study cohort; however, substantial overlap exists.

Materials and Methods

Patients

Institutional review board approval was not required, and the need for informed consent was waived.

Between October 2008 and March 2010, 130 consecutive patients underwent MR-guided prostate biopsy of CSRs seen on previous diagnostic 3-T MR prostate images and were eligible for inclusion this retrospective study. MR-guided biopsy was performed in male patients with *(a)* an elevated PSA level (>4 ng/mL), *(b)* family history of PCa, *(c)* suspicion for PCa based on diagnostic MR examination of the pelvis, and *(d)* at least one negative transrectal US biopsy session. Inclusion criterion for this study was that a DW sequence was performed at both the diagnostic MR examination and the MR-guided biopsy examination (Fig 1). Exclusion criteria for this study were patients with suspicion of recurrent PCa after therapy (prostatectomy, radiation therapy, chemotherapy, cryosurgery, or high-intensity focused ultrasound therapy), and biopsy specimens that could not be categorized within the following histopathologic groups: normal prostate tissue, prostatitis, low-grade PCa (Gleason grade components 2 or 3) and high-grade PCa (Gleason grade components 4 or 5). Eighty-eight patients met the inclusion criteria and were included for further analysis.

Diagnostic MR Imaging

Before the biopsy procedure, a diagnostic MR examination was performed with a 3-T MR imager (Trio Tim; Siemens, Erlangen, Germany). This multiparametric detection and localization examination consisted of T2-weighted imaging, DW imaging, and dynamic contrast-enhanced MR imaging (36).

Published online before print
10.1148/radiol.12111683 **Content code:** GU

Radiology 2013; 267:164–172

Abbreviations:
ADC = apparent diffusion coefficient
CG = central gland
CSR = cancer-suspicious region
DW = diffusion weighted
FISP = fast imaging with steady precession
PCa = prostate cancer
PSA = prostate-specific antigen
PZ = peripheral zone

Author contributions:
Guarantors of integrity of entire study, K.N.A.N., M.G.S., J.O.B., J.J.F.; study concepts/study design or data acquisition or data analysis/interpretation, all authors; manuscript drafting or manuscript revision for important intellectual content, all authors; approval of final version of submitted manuscript, all authors; literature research, K.N.A.N., M.G.S., B.t.H.; clinical studies, K.N.A.N., M.G.S., T.H., J.O.B., J.J.F.; experimental studies, K.N.A.N., M.G.S., T.H., G.J.S.L., B.t.H.; statistical analysis, K.N.A.N., M.G.S., G.J.S.L., C.M.A.H., J.J.F.; and manuscript editing, K.N.A.N., M.G.S., G.J.S.L., C.M.A.H., B.t.H., J.O.B., J.J.F.

Conflicts of interest are listed at the end of this article.

Peristalsis was suppressed with an intramuscular administration of 20 mg butylscopolaminebromide (Buscopan; Boehringer-Ingelheim, Ingelheim, Germany) and 1 mg of glucagon (Glucagen; Nordisk, Gentofte, Denmark).

The imaging protocol included the following sequences (Table 1): First, a T2-weighted turbo spin-echo sequence was performed in three planes. Second, a single-shot echo-planar imaging sequence with diffusion modules and fat suppression pulses was performed. The imager software automatically calculated ADC maps. Third, three-dimensional T1-weighted spoiled gradient-echo images were acquired during an intravenous bolus injection of a paramagnetic gadolinium chelate, 0.1 mmol of gadopentetate dimeglumine (Dotarem; Guerbet, Paris, France) per kilogram of body weight, which was administered with a power injector (Spectris Medrad, Warrendale) at 2.5 mL/sec and followed by a 15-mL saline flush. With this sequence, a three-dimensional volume covering the entire prostate was acquired every 2.5 seconds during 210 seconds, with the same positioning angle and center as the transverse T2-weighted sequence. Before contrast material injection, the same transverse three-dimensional T1-weighted gradient-echo sequence (with the exception of repetition time msec/echo time msec, 800/1.6, and flip angle of 8°) was used to obtain proton-density images, with identical positioning to allow calculation of the relative gadolinium chelate concentration curves.

Diagnostic MR Image Interpretation

The diagnostic MR images were analyzed with an in-house developed analytical software workstation that calculated the dynamic contrast-enhanced MR imaging parameters and projected these parameters as color overlay maps over the T2-weighted images (37,38). Images of all patients were read by two radiologists in consensus with 15 years (J.O.B.) and 7 years (J.J.F.) of experience in prostate MR imaging. The high-spatial-resolution, axial T2-weighted images were used as basis for evaluation of the prostate, and all other functional imaging modalities were interpreted in relation to these. On T2-weighted images, the generally known PCa detection criteria were used to determine CSRs. These

Figure 1

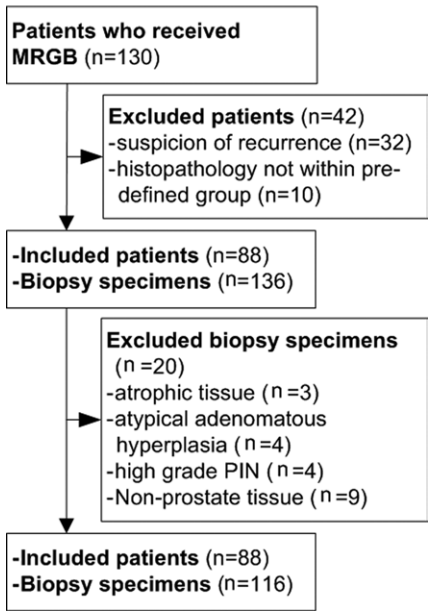

Figure 1: Study flow diagram. *MRGB* = MR-guided prostate biopsy; *PIN* = prostatic intraepithelial neoplasia.

Table 1

Imaging Parameters

Imaging Protocol	Sequence	Repetition Time (msec)	Echo Time (msec)	Flip Angle (degrees)	Voxel Size (mm^3)	*b* Values (sec/mm^2)	Temporal Resolution (sec)
Diagnostic MR imaging session							
T2 weighted	Axial turbo spin-echo	3620	116	180	0.4 × 0.4 × 3.0	NA	NA
DW	Single-shot echo-planar with diffusion modules and fat suppression pulses	2500	91		1.5 × 1.5 × 3.0	0, 50, 500, and 800	NA
DCE	3D T1-weighted spoiled gradient echo	34	1.6	14	1.5 × 1.5 × 4.0	NA	2.5
Proton density	3D T1-weighted spoiled gradient echo	800	1.6	8	1.5 × 1.5 × 4.0	NA	NA
MR-guided biopsy session							
True FISP	True FISP	4.48	2.24	70	1.1 × 1.1 × 3.0	NA	NA
DW	Single-shot echo-planar with diffusion modules and fat suppression pulses	2000	67		1.8 × 1.8 × 4.0	0, 100, 500, and 800	
T2 weighted	Axial turbo spin-echo	3620	104	120	0.8 × 0.8 × .0	NA	NA

Note.—DCE = dynamic contrast enhanced, NA = not applicable, 3D = three dimensional.

included low-signal-intensity areas in the peripheral zone (PZ) and/or a homogeneous low T2 signal intensity area with ill-defined margins or a lenticular shape within the CG (39). After identification of CSRs on T2-weighted images, the ADC maps and multiparametric dynamic contrast-enhanced MR imaging color maps transfer constant (K^{trans}), extravascular extracellular volume (v_e), rate constant (K_{ep}), and washout were analyzed in a color overlay mode on the T2-weighted images. The generally known features of PCa on dynamic contrast-enhanced MR images (13,40) (high v_e, K^{trans}, K_{ep}, and negative washout) and areas of restriction on ADC maps (especially in the PZ and CG) were used to identify CSRs qualitatively (38). Additionally, after the functional data from DW and dynamic contrast-enhanced MR imaging were evaluated in relation to the CSR findings on the T2-weigthed images, the DW and dynamic contrast-enhanced MR images were viewed separately and in combination to determine additional CSRs not evident on T2-weighted images. Finally, the information from all the imaging modalities were combined and used to determine the CSRs within the PZ and CG of the prostate (38).

MR-guided Biopsy Protocol

In a second session, prostate biopsies were performed in the same MR imager with a dedicated MR-compatible biopsy device (Invivo, Schwerin, Germany) (38,41–43). As previously described, the patient was placed in a prone position and the rectally inserted needle sleeve was attached to the arm of the MR-compatible biopsy device. A pelvic phased-array coil was used for signal reception (36,38).

Identification of the CSR, determined during the initial MR examination, was achieved by using the following MR sequences (Table 1): First, an axial T2-weighted turbo spin-echo sequence was performed. Second, an axial DW sequence was performed with a single-shot echo-planar imaging sequence with diffusion modules and fat suppression pulses. Water diffusion in three directions was measured by using four *b* values. Finally, the imager software calculated ADC maps automatically (Fig 2).

After identification of the CSRs, adjustments were applied to the biopsy device to move the needle sleeve exactly toward a CSR (41,42). To control needle sleeve direction, T2-weighted true fast imaging with steady precession (FISP) images were acquired in the axial and sagittal direction. Biopsy was performed in all determined CSRs on the diagnostic MR images, even if they were not visible on the T2-weighted anatomic MR images obtained at the time of biopsy. In these cases, the DW MR images were used to move the needle sleeve toward the CSR.

After fixation of the needle sleeve in the correct position, one or more tissue samples were taken at the region with lowest ADCs in each CSR with an 18-gauge, fully automatic, core needle, double-shot biopsy gun (Invivo) with a needle length of 150 or 175 mm and tissue sampling core length of 17 mm. After obtaining a biopsy specimen, fast T2-weighted axial and sagittal true-FISP images were obtained with the needle left in situ.

MR Image Correlation

During the biopsy session, at least one biopsy specimen was obtained from each CSR. The biopsy specimen that was located in the most diffusion-restricted area of each CSR was selected for image analysis. This was performed by using the true-FISP confirmation image and the corresponding ADC map obtained during the biopsy session. Some patients had multiple CSRs. The CSRs of all patients were analyzed without knowledge of the histopathologic outcomes. MR images of the biopsy specimens were analyzed with an in-house developed analytical software workstation (37). The calculated ADC maps were projected on the postbiopsy T2-weighted true-FISP images (confirmation image with the needle left in situ) to determine the biopsy location. By using this location, a region of interest was drawn manually with the size and extent of the most diffusion-restricted region on the ADC map, representing the biopsied CSR (Fig 3). In case of the absence of restricted diffusion on the ADC maps, a low-signal-intensity area on T2-weighted images was used to draw the region of interest. All regions of interest were annotated in consensus by two radiologists (T.H.,

Figure 2

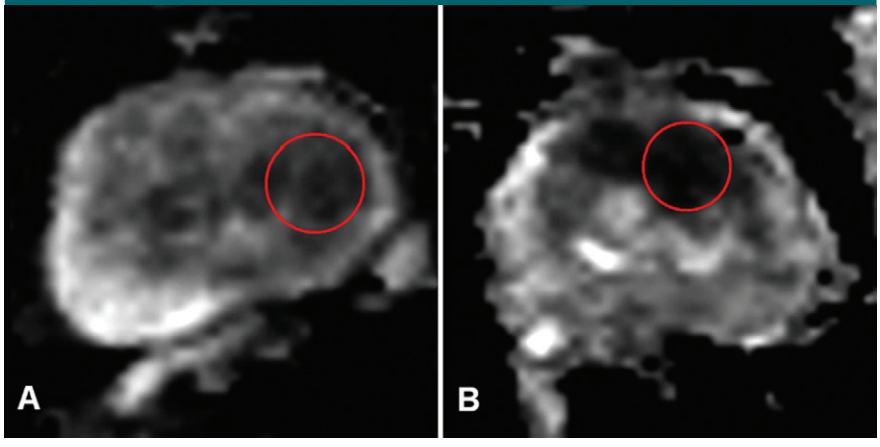

Figure 2: ADC maps calculated from a single-shot echo-planar DW image in three orthogonal diffusion gradients (2000/67; $b = 0$, 100, 500, and 800 sec/mm^2) in the axial plane in two men with a CSR in the CG. *A*, Image in a 72-year-old man (PSA = 22.1 ng/mL) shows a CSR (red circle) with a median ADC of 0.97×10^{-3} mm^2/sec. Histopathologic examination of the corresponding biopsy specimens revealed prostatitis. *B*, Image in a 65-year-old man (PSA = 30.0 ng/mL) shows a suspicious region (red circle) with a median ADC of 0.83×10^{-3} mm^2/sec. Histopathologic examination of this biopsy specimen revealed low-grade PCa (Gleason grade 3 + 3).

J.J.F.). Of each region of interest, the median and standard deviation of the ADC values were calculated (median size, 51; range 8–335 voxels). Multiple regions of interest were obtained in case a patient had multiple CSRs.

Histopathologic Evaluation

Biopsy specimens were processed by means of a routine fixation in formaldehyde, embedded in paraffin, and stained with hematoxylin-eosin before being evaluated by a pathologist for the presence of PCa or other benign pathologic lesions. Biopsy specimens with PCa were graded according to the 2005 ISUP Modified Gleason Grading System (44).

Statistical Analysis

A Mann-Whitney *U* test was performed to determine how ADC operates as a discriminatory test between prostatitis and CSRs. We have studied data summaries by region in addition to histopathologic grouping. The analyses were conducted by using linear mixed-effects regression models without autoregressive time-component, because in some patient multiple regions of interest were drawn. The significance level was set at a *P* value of less than .05. All analyses were performed with statistical software (SPSS, version 18.0.0; SPSS, Chicago, Ill).

Results

In our study, 88 of the 130 consecutive patients with CSRs on diagnostic MR images met the inclusion criteria and were included in our study (Table 2). These patients had one (n = 62), two (n = 24) or three CSRs (n = 2). A total of 136 MR-guided prostate biopsy specimens were obtained. Twenty biopsy specimens could not be categorized within the defined histopathologic groups (Table 2) and were excluded from further analysis. Consequently, 116 biopsy specimens were included and divided in four histopathologic classified groups: normal prostate tissue (32), prostatitis (42), low-grade PCa (25), and high-grade PCa (17). The 42 cancer-positive biopsy specimens were obtained from 39 patients. Patient and

Figure 3

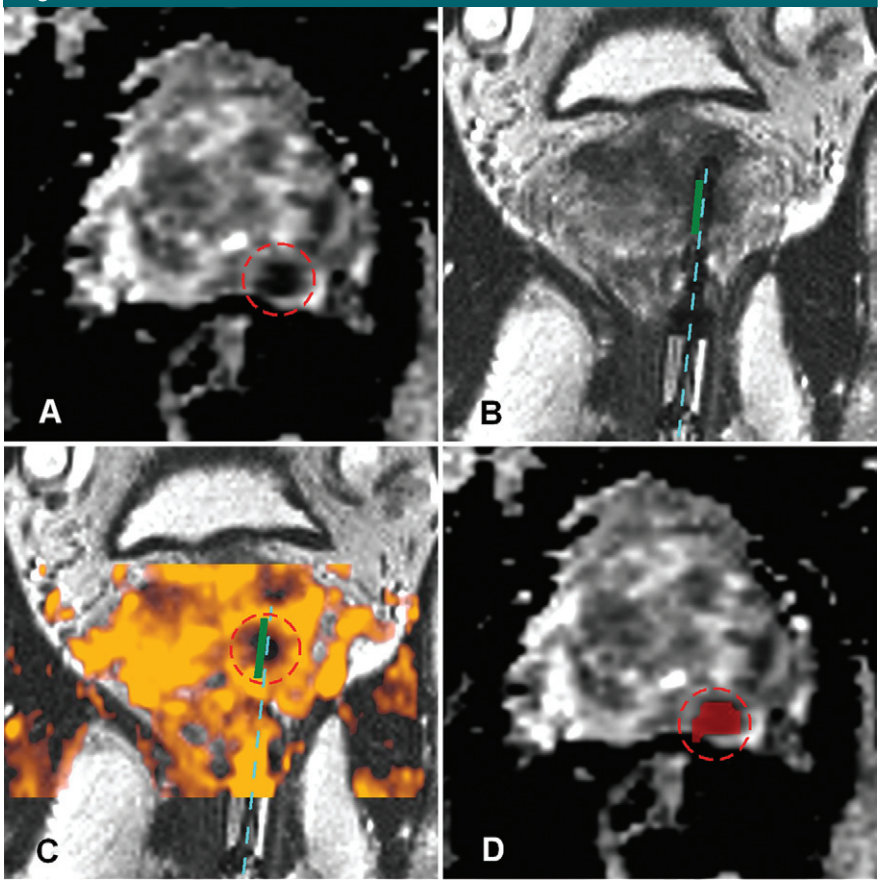

Figure 3: Images obtained in a 66-year-old man (PSA = 21.6 ng/mL) with a CSR in the PZ. Biopsy revealed a Gleason grade 3 + 3 PCa. *A*, The CSR (red circle) at prebiopsy MR imaging is visible on the ADC map, calculated from an axial single-shot echo-planar DW image by using three orthogonal diffusion gradients (2000/67; b = 0, 100, 500, and 800 sec/mm^2). *B*, Control T2-weighted true-FISP image (4.48/2.24) obtained during biopsy in axial and sagittal plane shows the position of the biopsy needle (dashed blue line) with a sampling core length of 17 mm (green line). *C*, After projection of the ADC map on the true-FISP image, *D*, a region of interest was drawn manually with the size and extent of the restricted diffusion region on the ADC map.

Table 2

Biopsy Findings Excluded from Analysis

Reason for Exclusion	No. Excluded
Excluded patients	42
Prostate treatment (prostatectomy, radiation therapy, chemotherapy, cryosurgery, or HIFU therapy)	32
Deviating biopsy specimens	10
Atrophic tissue	4
Atypical adenomatous hyperplasia	1
High-grade PIN	3
Nonprostate tissue	2
Excluded biopsy specimens of included patients	20
Atrophic tissue	3
Atypical adenomatous hyperplasia	4
High-grade PIN	4
Nonprostate tissue	9

Note.—Data are numbers of patients excluded or numbers of biopsy specimens excluded (among included patients). HIFU = high-intensity focused ultrasound, PIN = prostate intraepithelial neoplasia.

biopsy characteristics of these groups are shown in Table 3. In six cases, the determined CSRs on the initial diagnostic MR images were not visible on the MR images obtained at biopsy (hereafter, the "biopsy MR images"). Although not visible, the suspected area was biopsied. Furthermore, no new CSRs were seen on the biopsy MR images. Therefore, the numbers of CSRs on the diagnostic and biopsy MR images were equal. During the image analysis, 12 CSRs showed a low-signal-intensity area on T2-weigthed images and no restricted diffusion on the ADC maps, and 15 CSRs had an area of restricted diffusion without abnormality on the T2-weighted images. Discrepancies between the CSRs on the diagnostic MR images and the corresponding CSRs on the biopsy MR images were found in 5% (six of 116) of the biopsy specimens.

Biopsy specimens with normal prostate tissue, prostatitis, low-grade PCa, and high-grade PCa had a mean ADC of 1.22×10^{-3} mm^2/sec ± 0.21 (standard deviation), 1.08×10^{-3} mm^2/sec ± 0.18, 0.88×10^{-3} mm^2/sec ± 0.15, and 0.88×10^{-3} mm^2/sec ± 0.13, respectively (Fig 4, Table 4). The linear mixed-model analyses revealed significant differences between mean ADCs of the groups with normal prostate tissue and prostatitis (P = .002), the groups with prostatitis and low-grade PCa ($P < .001$), and the groups with prostatitis and high-grade PCa ($P < .001$). The difference between the mean ADCs of the groups with low-grade and high-grade PCa was not significant (P = .76).

Also, differences in mean ADCs between the three classified groups were analyzed for the PZ and CG. A total of 69 and 47 biopsy specimens were obtained from the PZ and CG, respectively. Median ADCs of the classified groups and regions are shown in Table 4. The linear mixed-model analyses showed a significant difference between the mean ADCs of the biopsy specimens with normal prostate tissue and prostatitis in the PZ (P = .012). This statistical analysis was not performed for the CG, because the number of biopsy specimens with normal prostate tissue in the CG was too low (n = 9). In both PZ and CG, however, significant differences in

Table 3

Patient and Biopsy Characteristics

Characteristic	All Patients	Normal Tissue	Prostatitis	Low-grade PCa	High-grade PCa	Excluded Tissue
No. of included patients	88					
No. of included biopsy specimens	116	32	42	25	17	
No. of excluded biopsy specimens	20					20
Median no. of previous negative transrectal US-guided biopsy sessions	2 (0–6)	2 (0–6)	2 (1–5)	2 (0–5)	3 (1–4)	
Mean age (y)	63 (44–76)	62 (52–76)	63 (50–73)	63 (44–72)	67 (56–73)	
Median PSA (ng/mL)	11.0 (0.1–58.0)	11.1 (0.8–36.0)	10.9 (0.1–30.2)	10.0 (1.2–51.0)	15.0 (18.0–51.0)	
Median prostate volume (mL)	49 (18–263)	79 (20–108)	55 (30–263)	40 (18–107)	42 (25–98)	
Median time between MR-guided biopsy and initial diagnostic MR examination (wk)	8.9 (0.0–31.7)	8.7 (2.3–21.0)	8.7 (0.0–31.7)	10.0 (2.1–31.4)	8.3 (3.1–16.4)	
Location of CSRs						
PZ	69	23	27	14	5	
CG	47	9	15	11	12	
No. of excluded biopsy specimens among the included patients						
Atrophic tissue						3
Atypical adenomatous hyperplasia						4
High-grade PIN						4
Nonprostate tissue						9
Low-grade PCa Gleason score						
2 + 3				2		
3 + 2				1		
3 + 3				22		
High-grade PCa Gleason score						
3 + 4					12	
3 + 5					1	
4 + 3					3	
4 + 5					1	

Note.—Data are numbers of patients or biopsy specimens, and numbers in parentheses are the range. PIN = prostate intraepithelial neoplasia.

mean ADCs were found between the groups with prostatitis and low-grade PCa (PZ: $P = .01$, CG: $P < .001$). Furthermore, a significant difference was revealed between the groups with prostatitis and high-grade PCa in the PZ ($P = .016$). The difference between the mean ADCs of the groups with low-grade PCa and high-grade PCa in PZ was not significant ($P = .84$). Again, the numbers in the group with high-grade PCa in the CG was too low ($n = 5$) to use for statistical analyses.

Discussion

In our study cohort, we found differences between mean ADCs of biopsy specimens with prostatitis and low- and high-grade PCa ($P < .001$), even though there was a high degree of overlap. It is questionable whether differences in mean ADCs of 0.14×10^{-3} mm^2/sec between the groups with PCa and prostatitis, although statistically significant, are also clinically useful. The overlap of ADCs between these two histopathologic groups hinders a reliable differentiation between prostatitis and PCa in routine clinical practice. Nevertheless, a CSR with a mean ADC of less than 0.75×10^{-3} mm^2/sec appears suspicious for PCa (see Fig 4) and a biopsy procedure might be recommended. Future studies will be needed that focus on the combined approach of functional imaging techniques to reduce the diagnostic overlap between prostatitis and PCa.

In recent years, several studies have demonstrated significant differences between the ADCs of malignant and benign prostate tissue by using transrectal US–guided biopsy (22–27) or step-section specimens after prostatectomy as reference standard (31–34). In these previously described studies, mean ADCs for malignant and benign prostate tissue varied over a relatively broad range from 0.93×10^{-3} mm^2/sec to 1.38×10^{-3} mm^2/sec and from 1.34×10^{-3} mm^2/sec to 1.96×10^{-3} mm^2/sec, respectively. However, in our study, mean ADCs were lower for both malignant (range, 0.78 to 0.90×10^{-3} mm^2/sec) and benign (range, 0.99 to 1.13×10^{-3} mm^2/sec) biopsy specimens. This may be explained by the fact that the biopsy specimens with normal prostate tissue were CSRs based on multiparametric MR imaging. The regions of interest of

Figure 4

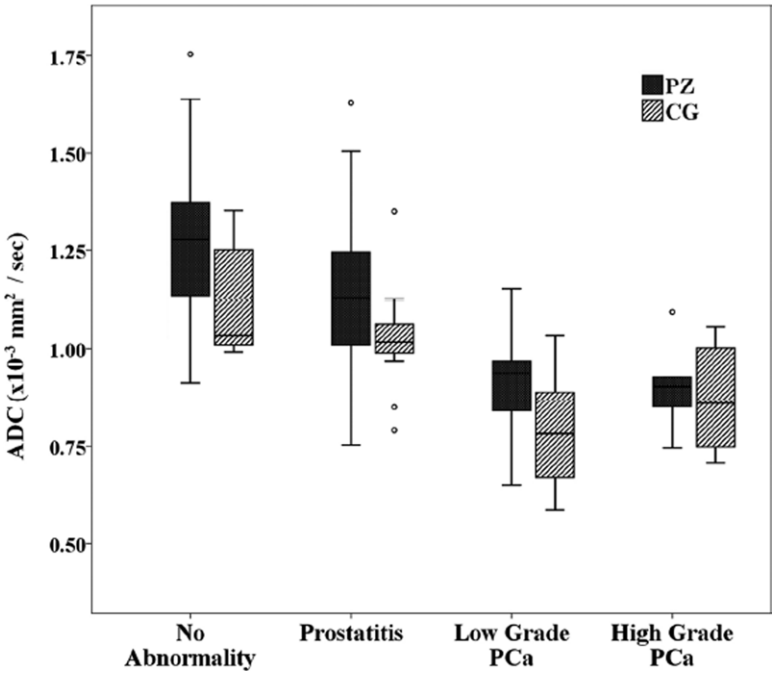

Figure 4: Box-and-whisker plots for the DW imaging of the suspicious areas according to histologic diagnosis of normal prostate, prostatitis, and low- and high-grade PCa in the PZ, CG, and combined PZ and CG. Center horizontal line = median, bottom and top edges of box = 25th and 75th percentiles, vertical line = range of data.

Table 4

Mean ADCs of the Histopathologic Groups

	PZ		CG	
Group	Mean ADC ± Standard Deviation*	No. of Specimens	Mean ADC ± Standard Deviation*	No. of Specimens
Normal tissue	1.28 ± 0.22†	23	1.03 ± 0.15‡	9
Prostatitis	1.13 ± 0.20	27	1.02 ± 0.13	15
Low-grade PCa	0.94 ± 0.13†	14	0.78 ± 0.15†	11
High-grade PCa	0.90 ± 0.13‡	5	0.86 ± 0.13†	12

* Unit of measure is $\times 10^{-3}$ mm^2/sec.

† Mean in this histopathologic group is significantly different from that of the reference group, prostatitis ($P < .05$).

‡ Number of biopsy specimens of this group is too low for reliable statistical analysis.

the previously described studies were annotated without abnormalities on multiparametric MR images. This could have resulted in relatively higher ADCs compared with our study.

The PCa detection rate of our study (44%) is lower compared with previous reports (52%–59%) (41,43,45). This could be explained by inclusion of one patient with a low PSA level (0.1 ng/mL) and patients with a positive family history of PCa.

A limited number of studies have assessed the histopathologic findings of CSRs on ADC maps with step-section specimens after prostatectomy (31–34). It is difficult to correlate the ADC maps with the corresponding histologic slices, since deformation and shrinkage of the prostate may occur after prostatectomy. Furthermore, all these studies have annotated the CSRs on ADC maps according to step-section specimens of the prostate.

In our study, the time interval between the initial diagnostic MR examination and the biopsy session ranged from 0 to 32 weeks. Discrepancies between the CSRs on the diagnostic MR images and the corresponding CSRs on the biopsy MR images were found in 5% (six of 116) of the biopsy specimens. However, all determined CSRs on the diagnostic MR images underwent biopsy, even if they were not visible on the biopsy MR images. The image analyses were not negatively affected by large time intervals, because the biopsy MR images were used to determine the ADCs of the CSRs, instead of the diagnostic MR images. These biopsy MR images were obtained on the same day of the biopsy session. Therefore, growth or shrinkage of the CSR was minimized.

Our study had a number of limitations First, during manipulation of the needle sleeve, the prostate may have moved (ie, due to patient motion, peristaltic movement, and/or bladder filling). It is therefore imaginable that the ADC map, obtained before the needle sleeve manipulation, does not exactly match with the confirmation image on which the needle is left in situ. During the image analyses, these movements were corrected manually by using anatomic landmarks such as cysts, calcifications, and femoral head and pelvic bones around the prostate. Advanced registration software using anatomic landmarks may help to overcome these discrepancies (46).

Second, the spatial resolution of DW imaging was limited (1.8 × 1.8 mm). This may result in missing CSRs with a diameter smaller than approximately 4–5 mm. Conversely, the diameter of an 18-gauge biopsy needle, and the corresponding biopsy specimen, was approximately 1.0 mm. However, this titanium needle causes image artifacts on post-biopsy true-FISP images with a diameter of approximately 6 mm. Even if the spatial resolution of DW imaging can be improved in future, the accuracy of the determination of the position of the biopsy needle will likely remain limited due to these needle artifacts. In the future these may be overcome by using novel material for needle manufacture.

In biopsy specimens obtained in patients with PCa, the entire specimen may not contain PCa. In our study, we did not include tumor biopsy volumetry. Because the histopathologic reports did not describe the localization of the cancerous components in the biopsy specimen, we have disregarded the volume percentage. However, this limitation could have influenced the accuracy of the measurements. The change in the diagnostic MR imaging protocol during the study period and the differences between the diagnostic and biopsy protocol may have influenced lesion detection.

In conclusion, DW imaging is a noninvasive technique that demonstrates a difference in mean ADC between prostatitis and PCa by using MR-guided biopsy specimens as standard of reference, although its usability in clinical practice is limited due to a high degree of overlap.

Acknowledgment: We thank Maroeska Rovers, PhD, for her intellectual contribution to the manuscript.

Disclosures of Conflicts of Interest: K.N.A.N. No relevant conflicts of interest to disclose. **M.G.S.** No relevant conflicts of interest to disclose. **T.H.** No relevant conflicts of interest to disclose. **G.J.S.L.** Financial activities related to the present article: grant to institution from Dutch Cancer Society. Financial activities not related to the present article: none to disclose. Other relationships: none to disclose. **C.M.A.H.** No relevant conflicts of interest to disclose. **B.t.H.** No relevant conflicts of interest to disclose. **J.O.B.** Financial activities related to the present article: grant to institution from Dutch Cancer Society. Financial activities not related to the present article: none to disclose. Other relationships: none to disclose. **J.J.F.** No relevant conflicts of interest to disclose.

References

1. Hochreiter WW. The issue of prostate cancer evaluation in men with elevated prostate-specific antigen and chronic prostatitis. Andrologia 2008;40(2):130–133.
2. Battikhi MN, Hussein I. Age-specific reference ranges for prostate specific antigen-total and free in patients with prostatitis symptoms and patients at risk. Int Urol Nephrol 2006;38(3-4):559–564.
3. Ozden C, Ozdal OL, Guzel O, Han O, Seckin S, Memis A. The correlation between serum prostate specific antigen levels and asymptomatic inflammatory prostatitis. Int Urol Nephrol 2007;39(3):859–863.
4. Collins MM, Stafford RS, O'Leary MP, Barry MJ. How common is prostatitis? A national survey of physician visits. J Urol 1998; 159(4):1224–1228.
5. Yu KK, Hricak H. Imaging prostate cancer. Radiol Clin North Am 2000;38(1): 59–85, viii.
6. Fütterer JJ. MR imaging in local staging of prostate cancer. Eur J Radiol 2007; 63(3):328–334.
7. Engelbrecht MR, Jager GJ, Laheij RJ, Verbeek AL, van Lier HJ, Barentsz JO. Local staging of prostate cancer using magnetic resonance imaging: a meta-analysis. Eur Radiol 2002;12(9):2294–2302.
8. Scheidler J, Hricak H, Vigneron DB, et al. Prostate cancer: localization with three-dimensional proton MR spectroscopic imaging—clinicopathologic study. Radiology 1999;213(2):473–480.
9. Quint LE, Van Erp JS, Bland PH, et al. Prostate cancer: correlation of MR images with tissue optical density at pathologic examination. Radiology 1991;179(3):837–842.
10. Lovett K, Rifkin MD, McCue PA, Choi H. MR imaging characteristics of noncancerous lesions of the prostate. J Magn Reson Imaging 1992;2(1):35–39.
11. Schiebler ML, Tomaszewski JE, Bezzi M, et al. Prostatic carcinoma and benign prostatic hyperplasia: correlation of high-resolution MR and histopathologic findings. Radiology 1989;172(1):131–137.
12. Kim CK, Park BK, Kim B. Localization of prostate cancer using 3T MRI: comparison of T2-weighted and dynamic contrast-enhanced imaging. J Comput Assist Tomogr 2006;30(1):7–11.

13. Engelbrecht MR, Huisman HJ, Laheij RJ, et al. Discrimination of prostate cancer from normal peripheral zone and central gland tissue by using dynamic contrast-enhanced MR imaging. Radiology 2003;229(1): 248–254.

14. Yakar D, Hambrock T, Huisman H, et al. Feasibility of 3T dynamic contrast-enhanced magnetic resonance-guided biopsy in localizing local recurrence of prostate cancer after external beam radiation therapy. Invest Radiol 2010;45(3):121–125.

15. Heijmink SW, Scheenen TW, Fütterer JJ, et al. Prostate and lymph node proton magnetic resonance (MR) spectroscopic imaging with external array coils at 3 T to detect recurrent prostate cancer after radiation therapy. Invest Radiol 2007;42(6):420–427.

16. Wang L, Hricak H, Kattan MW, Chen HN, Scardino PT, Kuroiwa K. Prediction of organ-confined prostate cancer: incremental value of MR imaging and MR spectroscopic imaging to staging nomograms. Radiology 2006;238(2):597–603.

17. Kurhanewicz J, Vigneron DB, Hricak H, Narayan P, Carroll P, Nelson SJ. Three-dimensional H-1 MR spectroscopic imaging of the in situ human prostate with high (0.24-0.7-cm3) spatial resolution. Radiology 1996;198(3):795–805.

18. Gibbs P, Tozer DJ, Liney GP, Turnbull LW. Comparison of quantitative T2 mapping and diffusion-weighted imaging in the normal and pathologic prostate. Magn Reson Med 2001;46(6):1054–1058.

19. Issa B. In vivo measurement of the apparent diffusion coefficient in normal and malignant prostatic tissues using echo-planar imaging. J Magn Reson Imaging 2002;16(2):196–200.

20. Chan I, Wells W 3rd, Mulkern RV, et al. Detection of prostate cancer by integration of line-scan diffusion, T2-mapping and T2-weighted magnetic resonance imaging; a multichannel statistical classifier. Med Phys 2003;30(9):2390–2398.

21. Miao H, Fukatsu H, Ishigaki T. Prostate cancer detection with 3-T MRI: comparison of diffusion-weighted and T2-weighted imaging. Eur J Radiol 2007;61(2):297–302.

22. Pickles MD, Gibbs P, Sreenivas M, Turnbull LW. Diffusion-weighted imaging of normal and malignant prostate tissue at 3.0T. J Magn Reson Imaging 2006;23(2): 130–134.

23. Tanimoto A, Nakashima J, Kohno H, Shinmoto H, Kuribayashi S. Prostate cancer screening: the clinical value of diffusion-weighted imaging and dynamic MR imaging in combination with T2-weighted imaging. J Magn Reson Imaging 2007;25(1): 146–152.

24. Shimofusa R, Fujimoto H, Akamata H, et al. Diffusion-weighted imaging of prostate cancer. J Comput Assist Tomogr 2005;29(2): 149–153.

25. Hosseinzadeh K, Schwarz SD. Endorectal diffusion-weighted imaging in prostate cancer to differentiate malignant and benign peripheral zone tissue. J Magn Reson Imaging 2004;20(4):654–661.

26. Sato C, Naganawa S, Nakamura T, et al. Differentiation of noncancerous tissue and cancer lesions by apparent diffusion coefficient values in transition and peripheral zones of the prostate. J Magn Reson Imaging 2005;21(3):258–262.

27. Tamada T, Sone T, Jo Y, et al. Apparent diffusion coefficient values in peripheral and transition zones of the prostate: comparison between normal and malignant prostatic tissues and correlation with histologic grade. J Magn Reson Imaging 2008;28(3): 720–726.

28. Stewart CS, Leibovich BC, Weaver AL, Lieber MM. Prostate cancer diagnosis using a saturation needle biopsy technique after previous negative sextant biopsies. J Urol 2001;166(1):86–91; discussion 91–92.

29. Salomon L, Colombel M, Patard JJ, et al. Value of ultrasound-guided systematic sextant biopsies in prostate tumor mapping. Eur Urol 1999;35(4):289–293.

30. Amsellem-Ouazana D, Younes P, Conquy S, et al. Negative prostatic biopsies in patients with a high risk of prostate cancer. Is the combination of endorectal MRI and magnetic resonance spectroscopy imaging (MRSI) a useful tool? A preliminary study. Eur Urol 2005;47(5):582–586.

31. Yoshimitsu K, Kiyoshima K, Irie H, et al. Usefulness of apparent diffusion coefficient map in diagnosing prostate carcinoma: correlation with stepwise histopathology. J Magn Reson Imaging 2008;27(1): 132–139.

32. Kim CK, Park BK, Lee HM, Kwon GY. Value of diffusion-weighted imaging for the prediction of prostate cancer location at 3T using a phased-array coil: preliminary results. Invest Radiol 2007;42(12): 842–847.

33. Van As N, Charles-Edwards E, Jackson A, et al. Correlation of diffusion-weighted MRI with whole mount radical prostatectomy specimens. Br J Radiol 2008;81(966): 456–462.

34. Hambrock T, Somford DM, Huisman HJ, et al. Relationship between apparent diffusion coefficients at 3.0-T MR imaging and Gleason grade in peripheral zone prostate cancer. Radiology 2011;259(2):453–461.

35. Drew B, Jones EC, Reinsberg S, Yung AC, Goldenberg SL, Kozlowski P. Device for sectioning prostatectomy specimens to facilitate comparison between histology and in vivo MRI. J Magn Reson Imaging 2010; 32(4):992–996.

36. Yakar D, Hambrock T, Hoeks C, Barentsz JO, Fütterer JJ. Magnetic resonance-guided biopsy of the prostate: feasibility, technique, and clinical applications. Top Magn Reson Imaging 2008;19(6):291–295.

37. Vos PC, Hambrock T, Hulsbergen-van de Kaa CA, Fütterer JJ, Barentsz JO, Huisman HJ. Computerized analysis of prostate lesions in the peripheral zone using dynamic contrast enhanced MRI. Med Phys 2008;35(3):888–899.

38. Hambrock T, Fütterer JJ, Huisman HJ, et al. Thirty-two-channel coil 3T magnetic resonance-guided biopsies of prostate tumor suspicious regions identified on multimodality 3T magnetic resonance imaging: technique and feasibility. Invest Radiol 2008; 43(10):686–694.

39. Akin O, Sala E, Moskowitz CS, et al. Transition zone prostate cancers: features, detection, localization, and staging at endorectal MR imaging. Radiology 2006;239(3):784–792.

40. Fütterer JJ, Heijmink SW, Scheenen TW, et al. Prostate cancer localization with dynamic contrast-enhanced MR imaging and proton MR spectroscopic imaging. Radiology 2006;241(2):449–458.

41. Anastasiadis AG, Lichy MP, Nagele U, et al. MRI-guided biopsy of the prostate increases diagnostic performance in men with elevated or increasing PSA levels after previous negative TRUS biopsies. Eur Urol 2006;50(4):738–748; discussion 748–749.

42. Beyersdorff D, Winkel A, Hamm B, Lenk S, Loening SA, Taupitz M. MR imaging-guided prostate biopsy with a closed MR unit at 1.5 T: initial results. Radiology 2005; 234(2):576–581.

43. Hambrock T, Somford DM, Hoeks C, et al. Magnetic resonance imaging guided prostate biopsy in men with repeat negative biopsies and increased prostate specific antigen. J Urol 2010;183(2):520–527.

44. Epstein JI, Allsbrook WC Jr, Amin MB, Egevad LL; ISUP Grading Committee. The 2005 International Society of Urological Pathology (ISUP) consensus conference on Gleason grading of prostatic carcinoma. Am J Surg Pathol 2005;29(9): 1228–1242.

45. Roethke M, Anastasiadis AG, Lichy M, et al. MRI-guided prostate biopsy detects clinically significant cancer: analysis of a cohort of 100 patients after previous negative TRUS biopsy. World J Urol 2012;30(2):213–218.

46. Ukimura O, Hirahara N, Fujihara A, et al. Technique for a hybrid system of real-time transrectal ultrasound with preoperative magnetic resonance imaging in the guidance of targeted prostate biopsy. Int J Urol 2010;17(10):890–893.